Journal of Medicinal Chemistry

Article

Cite This: J. Med. Chem. 2019, 62, 7910−7922

pubs.acs.org/jmc

Structure Kinetics Relationships and Molecular Dynamics Show Crucial Role for Heterocycle Leaving Group in Irreversible Diacylglycerol Lipase Inhibitors

Antonius P.A. Janssen,[†] Jacob M.A. van Hengst,[†] Olivier J.M. Béquignon,[‡] Hui Deng,[†] Gerard J.P. van Westen,[‡] and Mario van der Stelt*,[†]

[†]Molecular Physiology, Leiden Institute of Chemistry, Leiden University, 2300RA Leiden, The Netherlands

[‡]Division of Drug Discovery and Safety, Leiden Academic Centre for Drug Research, Leiden University, P.O. Box 9502, 2300 RA Leiden, The Netherlands

Supporting Information

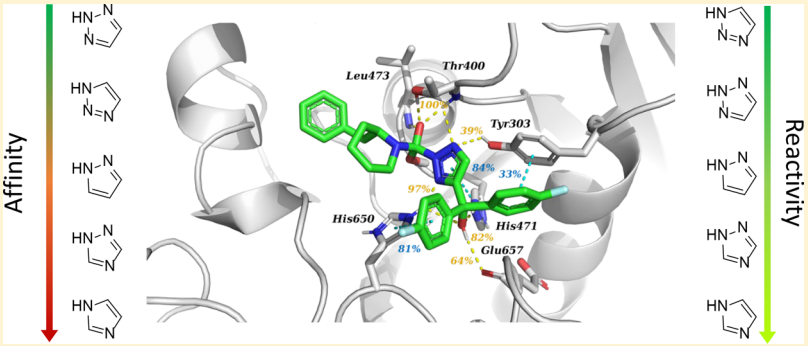

ABSTRACT: Drug discovery programs of covalent irreversible, mechanism-based enzyme inhibitors often focus on optimization of potency as determined by IC_{50}-values in biochemical assays. These assays do not allow the characterization of the binding activity (K_i) and reactivity (k_{inact}) as individual kinetic parameters of the covalent inhibitors. Here, we report the development of a kinetic substrate assay to study the influence of the acidity (pK_a) of heterocyclic leaving group of triazole urea derivatives as diacylglycerol lipase (DAGL)-α inhibitors. Surprisingly, we found that the reactivity of the inhibitors did not correlate with the pK_a of the leaving group, whereas the position of the nitrogen atoms in the heterocyclic core determined to a large extent the binding activity of the inhibitor. This finding was confirmed and clarified by molecular dynamics simulations on the covalently bound Michaelis−Menten complex. A deeper understanding of the binding properties of covalent serine hydrolase inhibitors is expected to aid in the discovery and development of more selective covalent inhibitors.

INTRODUCTION

The past decade has seen a renewed interest in the development of covalent inhibitors for several classes of drug targets, including the serine hydrolase and kinase superfamily.[1,2] Serine hydrolases perform a broad array of physiological functions and have diverse substrate preferences, but they all share a conserved catalytic nucleophilic serine residue. Serine hydrolases form a covalent acyl-enzyme intermediate, which can be exploited by irreversible, mechanism-based inhibitors. For example, PF-04457845 and ABX-1431 have entered clinical trials as fatty acid amide hydrolase (FAAH) and monoacylglycerol lipase (MAGL) inhibitors for the treatment of neurological diseases, respectively.[3−8] Covalent, irreversible inhibitors initially bind in a reversible fashion to the protein (i.e., the Michealis-Menten complex) followed by a time-dependent chemical reaction that inactivates the enzyme (Figure 1A,B).[9] The half-maximum inhibitory concentration (IC_{50}) for covalent inhibitors is dependent on a combination of binding affinity (K_i) and reactivity (k_{inact}). This fundamental dual aspect of covalent inhibition is often not taken into account during the optimization of covalent irreversible inhibitors, which is usually based on IC_{50} values.[2,10] This may lead to the prioritization of highly reactive molecules (large k_{inact}) based on their high potency.[11] Intrinsic high reactivity may, however, lead to a-specific binding to other members of the same enzyme family and unwanted adverse side effects as recently witnessed for BIA 10−2474.[12,13] Of note, the specificity constant $\left(\frac{k_{inact}}{K_i}\right)$ is sometimes employed to guide inhibitor optimization to avoid IC_{50}-values that are assay- and time-dependent.[14−16] The specificity constant is determined by measuring the observed rate constants (k_{obs}) using various inhibitor preincubation times but does not usually allow the independent determination and subsequent optimization of the affinity K_i, while

Received: April 26, 2019
Published: August 22, 2019

DOI: 10.1021/acs.jmedchem.9b00686
J. Med. Chem. 2019, 62, 7910−7922

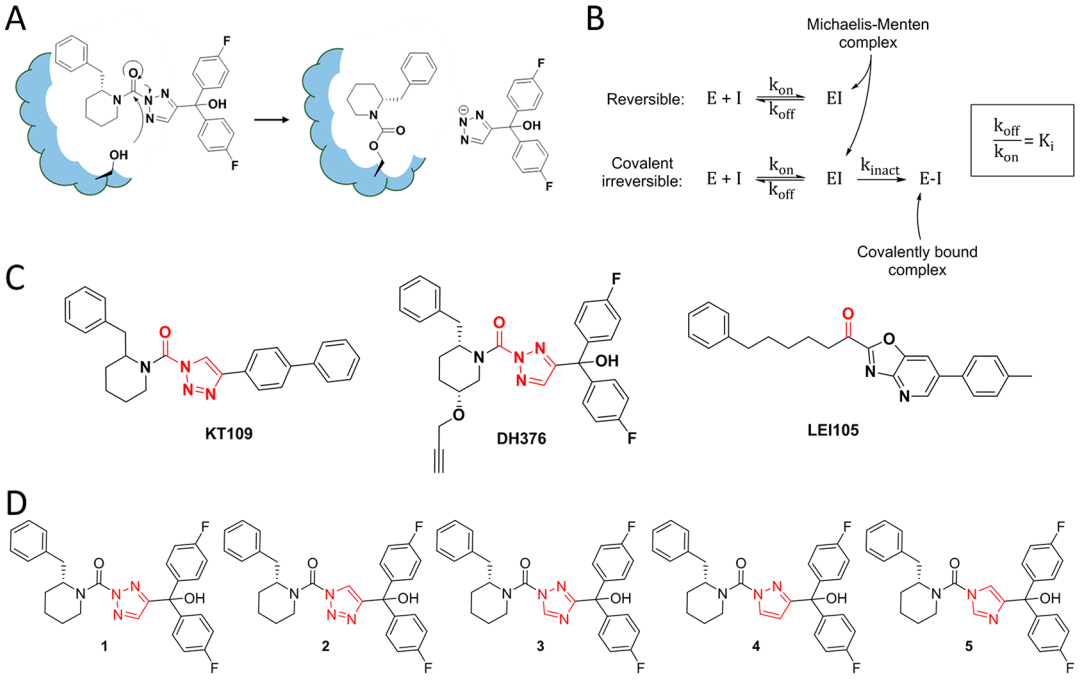

Figure 1. (A) Mechanism of action of mechanism-based triazole urea inhibitors for serine hydrolases. (B) The inhibition reactions for reversible and irreversible inhibition. E: enzyme, I: inhibitor, EI: Michaelis−Menten complex of E and I, E-I: covalently bound inhibitor-enzyme complex. (C) Recently published potent DAGL inhibitors. (D) Set of 5 inhibitors based on DH376 synthesized and characterized in this study.

minimizing the reactivity k_{inact}. Thus, alternative methods are required to determine K_i and k_{inact} in an independent manner.

Diacylglycerol lipases (DAGL) are serine hydrolases responsible for the synthesis of the endocannabinoid 2-arachidonoylglycerol (2-AG).[17] Modulation of DAGL activity holds therapeutic promise for the treatment of metabolic and neuroinflammatory diseases.[18−20] Several DAGL inhibitors, including KT109, DH376, and LEI105, have been developed (Figure 1C).[20−22] KT109 and DH376 belong to the class of triazole urea inhibitors, which are capable of irreversibly binding the catalytic serine through the formation of a stable carbamate adduct, thereby expelling a triazole-moiety as a leaving group (Figure 1A). This class of compounds has also shown merit as inhibitors for other serine hydrolases, such as α/β-hydrolase domain containing protein (ABHD) 6,[21] ABHD11,[23] DDHD domain-containing protein 2 (DDHD2),[24] and MAGL.[11,25] Structure activity studies of the DAGL (KT109 and DH376) and MAGL (JJKK-048) inhibitors have shown that the heterocyclic leaving group is crucially important for inhibitor activity.[11,26,27] The pK_a of the leaving group as determinant for the reactivity of the urea[28] was postulated to determine the activity of inhibitors.[11] The exact kinetic parameters of binding for these inhibitors have, however, thus far not been experimentally measured, thus the precise role of the triazole heterocycle in the inhibitor activity is unknown.

Here, we studied in detail the influence of the heterocycle in DAGL-α inhibitor DH376 on the binding and reactivity. To this end, we synthesized a coherent set of azole derivatives of DH376 to systematically investigate the role of the heterocycle in the activity of the inhibitor. Furthermore, we adapted a surrogate substrate assay of DAGL-α, which allowed us to independently measure K_i and k_{inact} of the new inhibitors. Surprisingly, we found that the azole has a crucial role in the formation of the Michaelis−Menten complex rather than in modulating the reactivity. To explain this finding, Molecular Dynamics was employed, which showed key interaction differences between compounds **1**−**5**. Taken together, the biological and computational data proves the importance of the heterocycle in binding affinity, not just reactivity.

RESULTS

To study the role of the azole heterocycle in the activity of the DAGL inhibitor DH376, a focused set of DH376 analogues was synthesized (**1**−**5**) (Figure 1D). Four different heterocycles (1,2,3-triazole, 1,2,4-triazole, pyrazole, and imidazole) and a regio-isomer of the 1,2,3-triazole were selected because they span a range of 5 orders of magnitude in pK_a.[29−31] The compounds were synthesized according to Scheme 1. The enantioselective synthetic route toward (*R*)-2-benzylpiperidine was adapted from Deng et al.[27] We replaced the low yielding transamination step, used to introduce an alkene at the free amine of **10**, by a simple alkylation with 4-bromobut-1-ene after nosyl protection of the amine (Scheme 1). This protected diene was subjected to ring-closing metathesis and, after deprotection, yielded **15** in a 3-fold higher overall yield than previously reported.[27] To synthesize the leaving group azole derivatives, a general synthetic route was devised featuring a Grignard reaction as core transformation to yield the di(*p*-fluorophenyl)methanol moiety in a single step from accessible azole esters (Scheme 1). For all but the imidazole derivative this worked without the introduction of any protecting group. Tritylation of the imidazole ethyl ester was necessary to avoid degradation during the Grignard reaction. Finally, the secondary amine **15** was first transformed in a carbamoyl chloride using triphosgene and subsequently reacted with the diphenyl azoles (**18**, **21**, **25**, and **29**), which furnished the inhibitors **1**−**5**.

To determine the binding kinetics of the inhibitors, we adapted the previously reported para-nitrophenolbutyrate

DOI: 10.1021/acs.jmedchem.9b00686
J. Med. Chem. 2019, 62, 7910−7922

Scheme 1. Synthesis of 1−5 Implementing the Optimized 9-Step Procedure for the Synthesis of (*R*)-2-Benzylpiperidine 15 from Commercially Available *N*-Boc-L-phenylalanine (6), Followed by the Coupling to the Biphenyl-Azole Leaving Groups Synthesized Using a General Grignard Reaction[a]

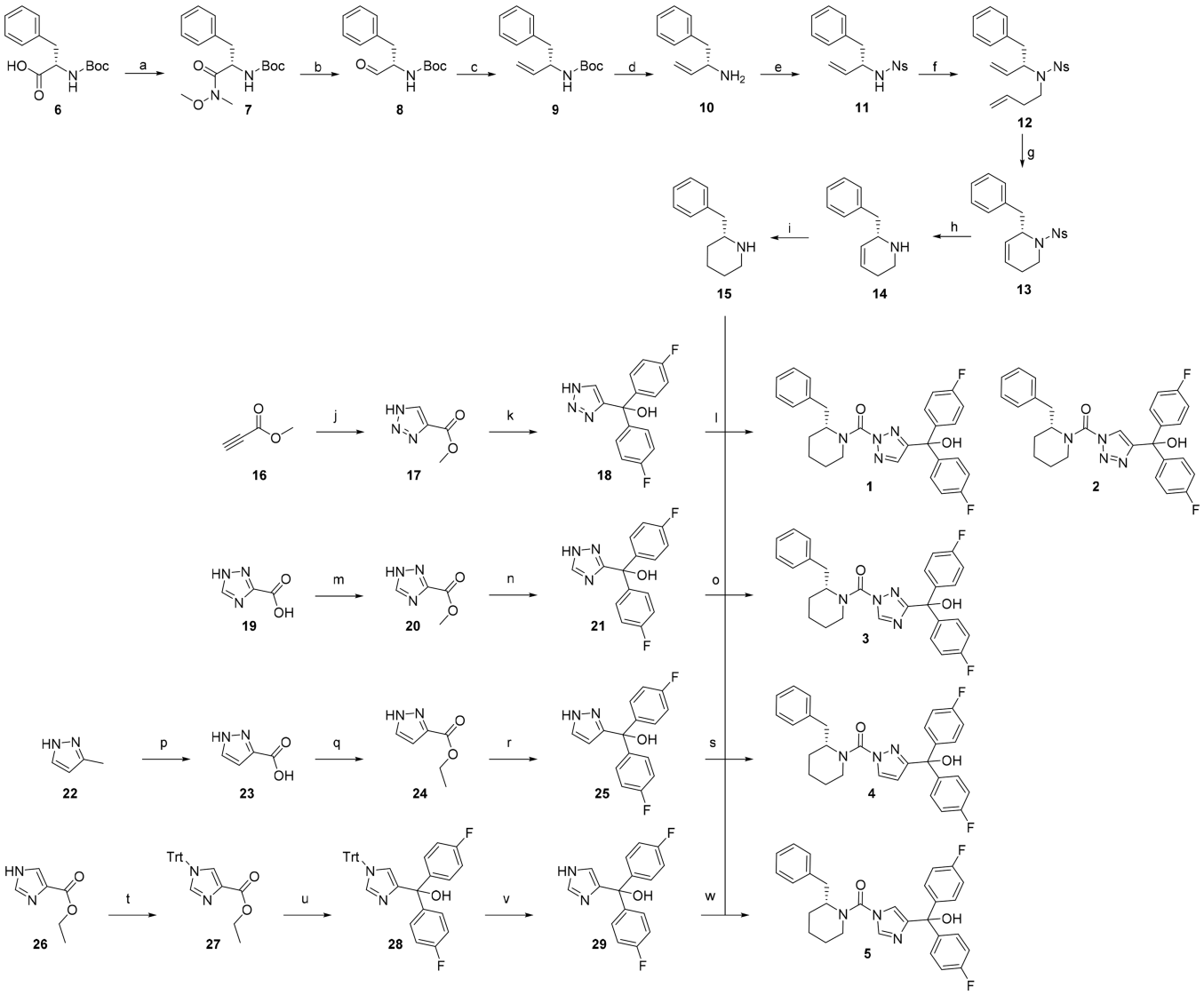

[a](a) *N*,*O*-di-Me-hydroxylamine·HCl, EDCI·HCl, DCM, 0 °C → RT, 92%;(b) $LiAlH_4$, THF, −20 °C, 96%; (c) $MeP(Ph)_3$·Br, KHMDS, THF, −78°C → RT, 56%; (d) HCl, MeOH/H_2O, quant.; (e) 2-NsCl, NEt_3, DMAP, DCM, 85%; (f) 4-bromobut-1-ene, K_2CO_3, DMF, 70 °C, 80%; (g) Grubbs' 1st gen., DCM, 40 °C, 62%; (h) PhSH, NaOH, ACN/H_2O, 50 °C, 99%; (i) $RuCl_3(H_2O)_3$, $NaBH_4$, DCE/MeOH, 87%; (j) TMS-N_3, 90 °C, 68%; (k) 4-F-PhMgBr, THF, 0 °C, 94%; (l) (i) **15**, triphosgene, Na_2CO_3, DCM; (ii) **18**, DIPEA, DMAP, THF, 66 °C, 1.5% (**1**) 1.2% (**2**); (m) MeOH, $SOCl_2$, 65 °C, 97%; (n) 4-F-PhMgBr, THF, 0 °C, 89%; (o) (i) **15**, triphosgene, Na_2CO_3, DCM; (ii) **21**, DIPEA, DMAP, THF, 66 °C, 35%; (p) $KMnO_4$, H_2O, 100 °C; (q) H_2SO_4, EtOH, 78 °C, 47% (two steps); (r) 4-F-PhMgBr, THF, 0 °C, 83%; (s) (i) **15**, triphosgene, Na_2CO_3, DCM; (ii) **25**, DIPEA, DMAP, THF, 66 °C, 21%; (t) TrCl, TEA, DCM, 0 °C → RT, 97%; (u) 4-F-PhMgBr, THF, 0 °C, 86%;(v) TFA, H_2O, DCM, 56%; (w) (i) **15**, triphosgene, Na_2CO_3, DCM; (ii) **29**, DIPEA, DMAP, THF, 66 °C, 27%.

(PNPB) assay.[32] A schematic overview of the changes made to the protocol is depicted in Figure 2A. The principal experimental difference is that the typical preincubation step with the inhibitors was omitted, and enzyme activity was continuously measured from the start (t = 0). To obtain a higher specific signal at early time points, the substrate concentration was increased to 600 μM. Furthermore, the enzyme was premixed with the assay buffer before addition to a 96-well plate, which contained a concentrated inhibitor and substrate, to minimize initial mixing effects. This yielded reproducible substrate conversion curves (Figure 2C−E).

Most available literature models, including the standard observed rate approximation (k_{obs}), assume that the enzyme concentration will not change during the incubation ($K_i \gg [E]$).[14,33−35] These models cannot, however, be applied to potent inhibitors, such as KT109 and DH376, that will decrease the enzyme concentration. Therefore, the kinetic model of Schwartz et al. was selected to fit to the substrate conversion curves.[10] In this model, DynaFit software is used for the numerical fitting of the full set of differential equations governing the substrate conversion curves without making the $K_i \gg [E]$ assumption.[10,36,37] The kinetic model from Schwartz et al. was slightly adapted to incorporate the spontaneous

DOI: 10.1021/acs.jmedchem.9b00686
J. Med. Chem. 2019, 62, 7910−7922

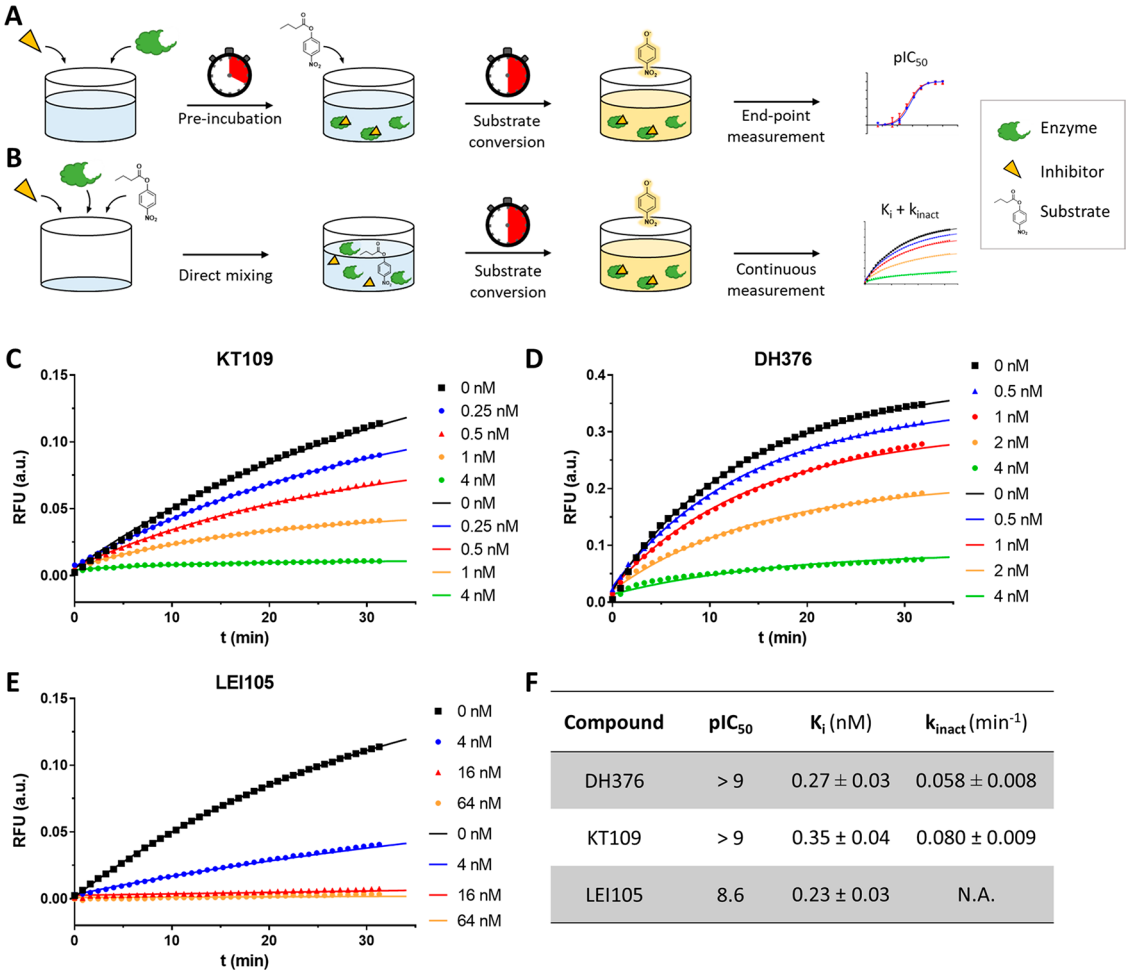

Compound	pIC_{50}	K_i (nM)	k_{inact} (min^{-1})
DH376	> 9	0.27 ± 0.03	0.058 ± 0.008
KT109	> 9	0.35 ± 0.04	0.080 ± 0.009
LEI105	8.6	0.23 ± 0.03	N.A.

Figure 2. Schematic overview of previously published PNP-butyrate based surrogate substrate assay (A) and the adapted workflow to determine binding kinetics (B). Kinetics of binding of KT109 (C), DH376 (D), and LEI105 (E); data fits are summarized in (F). For clarity, not all substrate conversion curves used for the curve fitting are shown. Markers denote measured absorbance, lines denote fitted model.

enzyme inactivation observed for blank measurements, where substrate depletion alone cannot explain the decrease in substrate conversion rate. As the substrate concentration was well below the predicted K_M, the one-step substrate conversion proposed by Schwartz et al. was maintained. Initial values for the required rate constants were derived from several preliminary experiments and were mostly left to be optimized by the algorithm (Figure S1).

The assay was validated using irreversible DAGL inhibitors (KT109 and DH376) and a reversible inhibitor (LEI105) (Figure 1C). All three inhibitors were previously found to be highly active with (sub)nanomolar potency (pIC_{50} = 8.6 to 9).[20,22,38] Using seven inhibitor concentrations around their reported IC_{50}-values, a set of substrate conversion curves was generated. These curves were fitted with DynaFit (Figure S1). The resulting fits and values for K_i and k_{inact} are shown in Figure 2. As was expected, the model does not find a fit for the k_{inact} value for the covalent but reversible inhibitor LEI105. The found K_i-values (all between 0.2 and 0.4 nM) were generally in line with the high potency described in literature, although LEI105 was somewhat more active than previously reported.[22] The inactivation rates for KT-109 and DH376 were similar (k_{inact} = ± 0.07 min^{-1}).

Next, we tested inhibitors **1**−**5** to determine the influence of the leaving group on their potency in the standard surrogate substrate assay. A large range in IC_{50}-values was observed (Figure 3A, Table 1). Both regioisomers **1** and **2** were low nanomolar inhibitors, whereas the 1,2,4-triazole (**3**) had a reduced potency (IC_{50} = 3.4 μM), and the imidazole (**5**) was inactive (IC_{50} > 10 μM). Pyrazole (**4**) had an intermediate potency with IC_{50} of 0.21 μM. The IC_{50}-values were used to guide the selection of inhibitor concentrations for the kinetic assay (Figure 3B, Table 1). For all but the imidazole compound **5**, we were able to determine the kinetic parameters. Intriguingly, the inactivation rates for **1** and **2** (k_{inact} = 0.22 and 0.32 min^{-1}, respectively) were 2−3 times higher than for KT109 and DH376, but they had a lower binding affinity (K_i = 10 and 339 nM, respectively). Unexpectedly, the inactivation rates for **3** and **4** were comparable to DH376 and KT109, whereas there is 10,000-fold difference in pK_a between these heterocycles (Table 1). Yet, the binding affinity of **3** and **4** was substantially reduced (K_i > 10 μM), thereby explaining their higher IC_{50}-values.

To understand the reasons behind this difference in binding, in silico experiments were carried out. In a two-step process, first covalent docking of compounds **1**−**5** to Ser472 of a previously developed homology model[32] was performed (Figure 4, Figure S3). Subsequently, dynamic evolution of the protein−ligands interactions was followed using molecular dynamics for all complexes (Figures S3−S7). The docked

DOI: 10.1021/acs.jmedchem.9b00686
J. Med. Chem. 2019, 62, 7910−7922

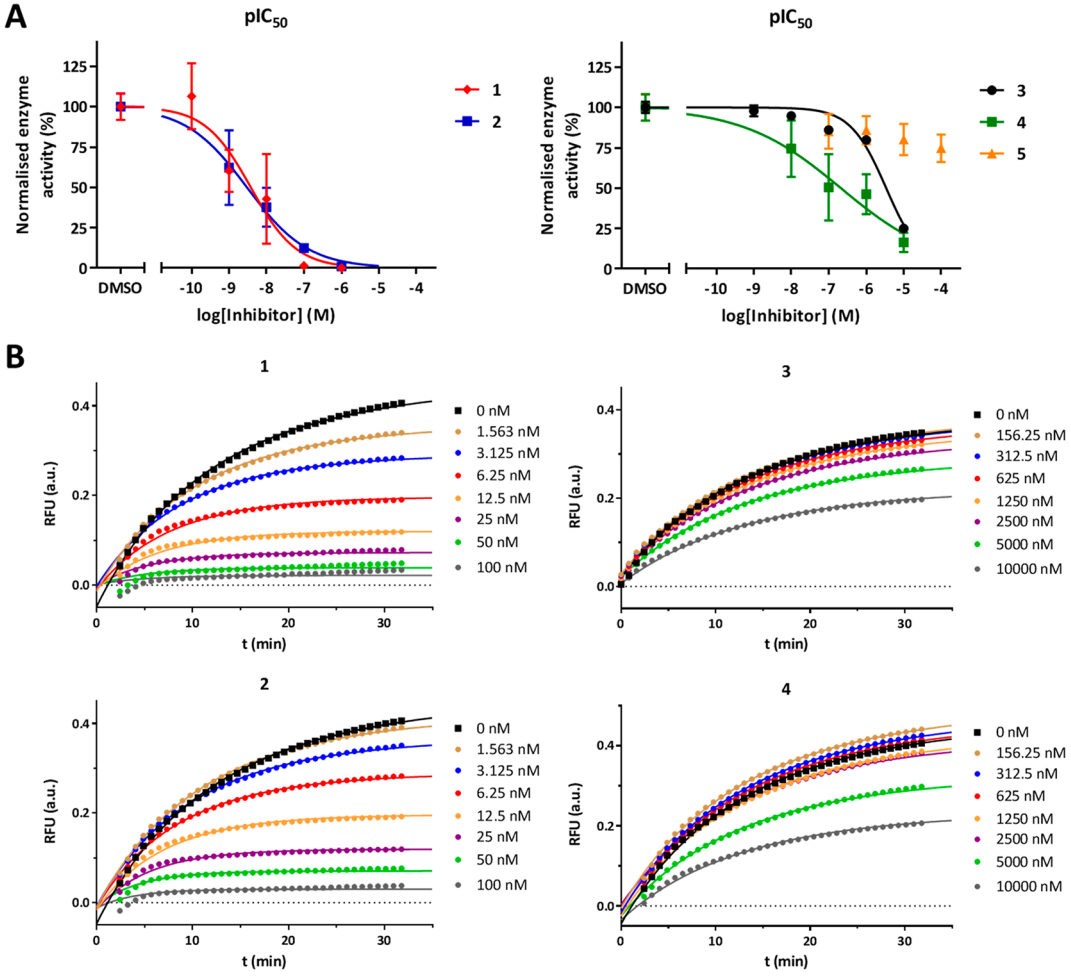

Figure 3. pIC_{50} determination of compounds **1**−**5** (A) and kinetic fits (B). All data points are measured as $n = 4$, positive controls (DMSO) as $n = 8$. Markers denote mean values, error bars denote the SEM, lines are fitted data models.

Table 1. Potency and Kinetic Parameters of the Focused Set of DH376 Derivatives 1−5

compound	pIC_{50}	K_i (nM)	k_{inact} (min^{-1})	pK_a
1	8.52 ± 0.27	10.4 ± 2.0	0.22 ± 0.03	9.3[31]
2	8.42 ± 0.28	339 ± 55	0.32 ± 0.04	9.3[31]
3	5.47 ± 0.07	13770 ± 910	0.075 ± 0.005	10.0[29]
4	6.68 ± 0.41	10800 ± 910	0.080 ± 0.005	14.2[30]
5	<4.5	N.D.	N.D.	14.4[30]

poses are assumed to reflect the Michaelis−Menten intermediate of the reaction displayed in Figure 1A. All complexes remained stable over the trajectories, and the negatively charged oxygen was continuously stabilized by the backbone of both Thr400 and Leu473 (Figures S4, S5, and S6). Assessment of the interactions through the frames of the dynamic evolution allowed the deconvolution of the observed binding behavior.

The observed high potency of **1** and **2** could be explained by the major hydrogen bonding with His650 (Figure 4A), similar as has been previously shown for α-positioned heterocycles for related serine hydrolases like FAAH and others.[39,40] The 1,2,3-triazoles are able to form this bond through the nitrogen in position 3. His650 is part of the catalytic triad and has been postulated to bind in this manner before, based on the covalent docking of α-ketoheterocycles in a homology model of DAGL-α.[41] Additionally, compound **1** forms a strong π-stacking interaction with His471 and a stable hydrogen bonding interaction with Tyr303, explaining the difference in potency observed with **2**, which forms a π-stacking interaction with His650, and less stable hydrogen bonding interaction with the nitrogen in position 1 and His471 (Figure S3). Compound **4** is also able to make this very stable hydrogen bonding between the nitrogen in position 2 and His650, potentially explaining the intermediate potency. Additionally, the hydroxyl interacts through a water-bridge with His471.

Interestingly, the 1,2,4-triazole and imidazole rings containing compounds (**3** and **5**) interact mostly only weakly through water bridging with His650. In many frames, these azoles are observed to rotate to a 90-degree angle which causes the loss of this interaction with His650. The further difference between the potencies of both these compounds may be explained by the capacity of nitrogen in position 2 in **3** to form water bridges with Tyr653 or Ser185 when adopting this 90-degree angle, which is not possible for the imidazole nitrogen in **5**.

DISCUSSION AND CONCLUSIONS

We developed a surrogate substrate based assay to determine the kinetic parameters of binding and reactivity of triazole urea inhibitors of the serine hydrolase DAGL-α. Having the ability to discern the kinetics of binding should enable the optimization of the affinity of the inhibitors for the enzyme,

DOI: 10.1021/acs.jmedchem.9b00686
J. Med. Chem. 2019, 62, 7910−7922

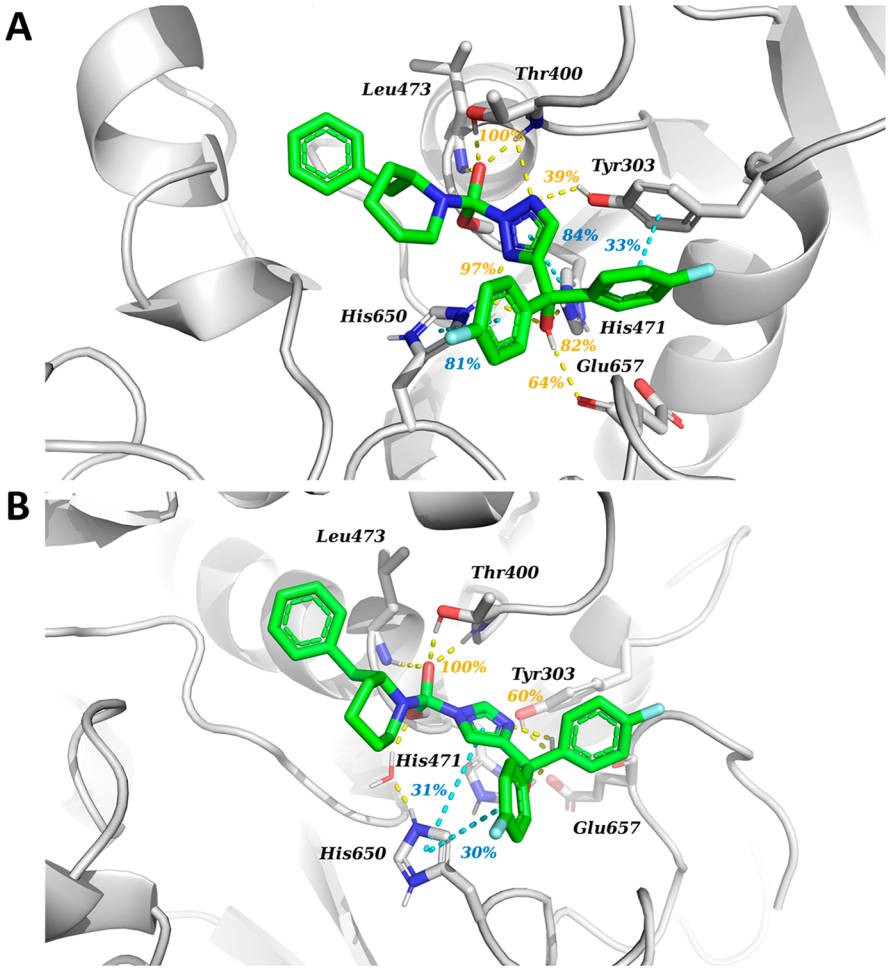

Figure 4. Representative frames of the molecular dynamics simulations showing highly potent 1,2,3-triazole **1** (A) and inactive imidazole **5** (B) bound to the DAGL-α homology model. Predominant interactions are shown, annotated with the percentage of frames showing this interaction (3 separate simulations, 100 frames each).

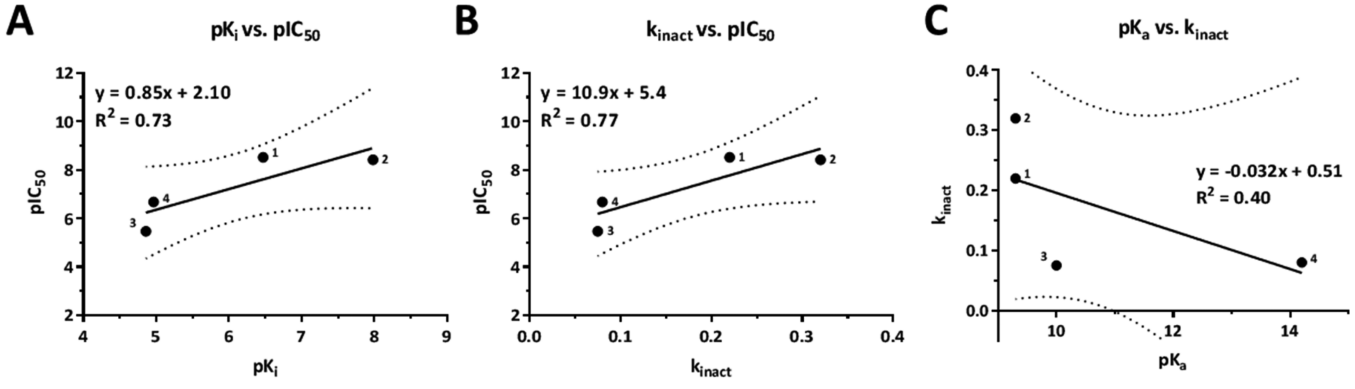

Figure 5. pIC_{50} correlates with both pK_i (A) and k_{inact} (B) but pK_a (C) does not correlate with reactivity for the inhibitors **1**−**4**. Dotted lines denote a 90% confidence interval.

the K_i, while controlling the reactivity k_{inact}, to minimize the off-target reactivity. The assay was validated using three well-characterized published DAGL inhibitors. Five DH376 derivatives were synthesized to study the role of the leaving group in the affinity and reactivity with DAGL-α. The IC_{50}-values correlated with the K_i and k_{inact} with a R^2 of 0.73 and 0.77, respectively (Figure 5A,B). The main reason for the large differences observed in IC_{50}-values for the five inhibitors was the strong reduction in binding affinity for the pyrazole and 1,2,4-triazole compounds compared to the 1,2,3-triazole inhibitors. In agreement with the known SAR,[27] **1** has a lower pIC_{50} than DH376. This is shown to be primarily due to a decrease in affinity, which signifies the role of the propargylether in DH376. The k_{inact} of DH376 was found to be slightly lower than **1**. No obvious explanation for this finding presents itself, but one could speculate the ether-oxygen to interfere in the hydrogen -bonding network needed for hydrolysis. Unexpectedly, it was shown that the 1,2,4-

DOI: 10.1021/acs.jmedchem.9b00686
J. Med. Chem. 2019, 62, 7910−7922

triazole **3** and pyrazole **4** inhibitors were as reactive as DH376 and KT109, which is in stark contrast to the 5 orders of magnitude difference in pK_a. This showed that the leaving group acidity does not correlate with the rate of inactivation k_{inact} (Figure 5C).

The striking difference in binding affinity was further explored using molecular dynamics. Compounds **1**−**5** were assumed to bind covalently to the catalytic serine upon Michaelis−Menten complex formation. The tetrahedral intermediate was evolved using molecular dynamics to analyze the interactions with the enzyme. The MD simulations also showed a large influence of the positioning and number of nitrogens in the ring, agreeing with the observations made in the kinetics assay. However, while these simulations are crucial for an understanding of the experimental data, the MD could not be used to study the reaction progress or (relative) speeds of the final covalent modification.

The assay presented here, in combination with the data analysis through numerical fitting, could be translated to work on a multitude of serine hydrolases. As long as a sensitive and robust (surrogate) substrate assay is available that can be interrogated in a time-dependent manner, it should in principle be possible to derive structure kinetics relationships. These relationships provide important insights into the mode of action and can aid in the optimization of covalent serine hydrolase inhibitors in an affinity directed manner. For the DAG lipase inhibitors, this may lead to more selective inhibitors more suitable for further in vivo target validation studies.

To conclude, we have developed a kinetic assay to study the influence of the heterocyclic core of triazole ureas as covalent, mechanism-based inhibitors of diacylglycerol lipase-α. We found that the pK_a of the leaving group did not correlate with the reactivity of the inhibitors but that the position of the nitrogen atom in the heterocycle is of importance in its binding affinity. These findings were in agreement with molecular dynamics simulations on covalently docked inhibitors in a homology model of DAGL-α. Detailed knowledge of structure kinetic relationships is expected to guide the optimization of more selective and well-balanced irreversible inhibitors of serine hydrolases.

EXPERIMENTAL SECTION

Chemical Biology Methods. *Cell Culture and Membrane Preparation.* HEK293T cells were grown in DMEM with stable glutamine and phenolred (PAA) with 10% New Born Calf serum, penicillin, and streptomycin. Cells were passaged every 2−3 days by resuspending in medium and seeding them to appropriate confluence. Membranes were prepared from transiently transfected HEK293T cells. One day prior to transfection 10^7 cells were seeded in a 15 cm Petri dish. Cells were transfected by the addition of a 3:1 mixture of polyethylenimine (60 μg) and plasmid DNA (20 μg) in 2 mL serum free medium. The medium was refreshed after 24 h, and after 72 h the cells were harvested by suspending them in 20 mL medium. The suspension was centrifuged for 10 min at 1000*g*, and the supernatant was removed. The cell pellet was stored at −80 °C until use.

Cell pellets were thawed on ice and suspended in lysis buffer (20 mM Hepes, 2 mM DTT, 0.25 M sucrose, 1 mM $MgCl_2$, 25 U/mL benzonase). The suspension was homogenized by polytrone (3× 7 s) and incubated for 30 min on ice. The suspension was subjected to ultracentrifugation (93,000*g*, 30 min, 4 °C, Beckman Coulter, Type Ti70 rotor) to yield the cytosolic fraction in the supernatant and the membrane fraction as a pellet. The pellet was resuspended in storage buffer (20 mM Hepes, 2 mM DTT). The protein concentration was determined with Quick Start Bradford assay (Biorad). The protein fractions were diluted to a total protein concentration of 1 mg/mL and stored in small aliquots at −80 °C until use.

Surrogate Substrate Assay. The biochemical mDAGL-α activity assay is based on the method previously described.[32] 100 μL reactions were performed in flat bottom Greiner 96-wells plates in a 50 mM pH 7.2 Hepes buffer. Membrane protein fractions from HEK293T cells transiently transfected with mDAGL-α (0.05 μg/μL final concentration) were used as a mDAGL-α source. Inhibitors were introduced in 2.5 μL DMSO. The mixtures were incubated for 20 min before 5.0 μL 6 mM PNP-butyrate (final concentration 0.3 mM) in 50% DMSO was added (final DMSO concentration 5.0%). Reactions were allowed to progress for 30 min at 20 °C before the OD (420 nm) was measured using a TECAN GENios plate reader. All experiments were performed at $N = 2$, $n = 2$ for experimental measurements, and $N = 2$, $n = 4$ for controls.

Data analysis: Z′-factor of each plate was determined for the validation of each experiment, using the following formula $Z' = 1 - 3(\sigma_{pc} + \sigma_{nc})/(\mu_{pc} - \mu_{nc})$. The OD from the positive control (pc: DAGL DMSO), and the negative control (nc: 10 μM THL) was used. Plates were accepted for further analysis when $Z' > 0.6$. Measurements were corrected for the average absorption of the negative control (10 μM THL). The average, standard deviation (SD) and standard error of mean (SEM) were calculated and normalized to the corrected positive control. Data was exported to Graphpad Prism 7.0 for the calculation of the pIC_{50} using a nonlinear dose−response analysis.

DynaFit Setup. DynaFit version 4 was used with an academic license. For batch processing, the command line interface was used. The raw data were preprocessed using Microsoft Excel 2016 and exported to tab delimited text files for use with DynaFit. Scripts were generated manually or using a purpose-made python script. An example DynaFit script is shown in Figure S1.

The contents of the header [task] follow directly from the DynaFit manual and simply state that the program should fit progress curves using the data supplied.

The section [mechanism] was built based on standard enzyme kinetics. The simplified hit and run (E + S → E + P) was used for the substrate conversion as the K_M of the surrogate substrate is too high to be determined reliably experimentally.[10,32] The additional enzyme degradation step (E → E*) was included as the progress rate curves for the DMSO blanks decreased more than could be explained by the reduction in substrate concentration (which is accounted for in the set of differential equations fitted).

The rate constants defined in [constants] were set empirically but are all left to be optimized. The exception is k_{on}, which is fixed to 100,000 μM^{-1} min^{-1}, but the variable itself is dependent on k_{off} (and vice versa), so only the ratio of the two (K_i) is physically meaningful in this experimental setup.

As the enzyme is obtained by overexpression in HEK293T cells, the exact concentration is unknown. Data from the previously published PNPB-based assay used for pIC_{50} determination indicate that the assay limit lies around 9, which puts the enzyme concentration at ±1 nM. It is left to be optimized by DynaFit.

The value for P given in the [responses] section is essentially the absorption coefficient of the converted surrogate substrate in AU·μM^{-1}, which was determined experimentally (Figure S2).

Molecular Dynamics. *Ligand Preparation.* Molecular structures of compounds **1** to **5** drawn with the specified chirality and prepared for docking using LigPrep[42] from Schrödinger. Default LigPrep settings were applied, using Epik[43] for the generation of ionization states of heteroatoms at pH = 7.0 ± 2.0 and the OPLS3e force-field[44] for geometry optimization. No tautomers were generated by the program resulting in one standardized structure per ligand.

Protein Preparation. A previously described homology model of DAGL-α[32] based on template with PDB code 1GT6 was prepared for docking using the Protein Preparation protocol from the Schrödinger 2018−4 suite with default settings. Ionization states of heteroatoms were generated with Epik at pH 7.0 ± 2.0, resulting in the protonation of the imidazole ring of His471 and His650.

DOI: 10.1021/acs.jmedchem.9b00686
J. Med. Chem. 2019, 62, 7910−7922

Covalent Docking. Covalent docking of the prepared compounds to Ser 472 was performed using the Schrödinger 2018−3 suite[45] with standard settings, generating one pose per compound. Docked ligands were confined to the enclosing box defined by the following residues: Tyr303, Gly399, Thr400, Thr408, Asp409, Met432, His471, Ser472, Leu473, Leu647, His650, Leu651, and Gly658.

Molecular Dynamics. Each protein−ligand complex was then subjected to molecular dynamics using Desmond Molecular Dynamics System from Schrödinger.[46] The system was set up using default settings, water solvent model SPC,[47] and OPLS3 force field.[44] Simulations were performed in triplicate at 300 K and 1.01 bar using hydrogen mass repartitioning with a runtime of 300 ns per run.

Chemistry. *General Remarks.* All reactions were performed using oven- or flame-dried glassware and dry (molecular sieves) solvents. Reagents were purchased from Alfa Aesar, Sigma-Aldrich, Acros, and Merck and used without further purification unless noted otherwise. All moisture sensitive reactions were performed under an argon or nitrogen atmosphere.

^{1}H and ^{13}C NMR spectra were recorded on a Bruker DPX-300 (300 MHz), AV-400 (400 MHz), or DRX-500 (500 MHz). Used software for interpretation of NMR-data was Bruker TopSpin 1.3 and MestreNova 11.0. Chemical shift values are reported in ppm with tetramethylsilane or solvent resonance as the internal standard ($CDCl_3$: δ 7.26 for ^{1}H, δ 77.16 for ^{13}C; ACN-*d*3: δ 1.94 for ^{1}H, δ 1.32 for ^{13}C; MeOD: δ 3.31 for ^{1}H, δ 49.00 for ^{13}C).[48] Data are reported as follows: chemical shifts (δ), multiplicity (s = singlet, d = doublet, dd = double doublet, td = triple doublet, t = triplet, q = quartet, bs = broad singlet, and m = multiplet), coupling constants *J* (Hz), and integration.

Liquid chromatography was performed on a Finnigan Surveyor LC/MS system, equipped with a C18 column. Final compound purity was ≥ 95% as determined by LC/MS; analytical traces are included in the Supporting Information. Flash chromatography was performed using SiliCycle silica gel type SiliaFlash P60 (230−400 mesh). TLC analysis was performed on Merck silica gel 60/Kieselguhr F254, 0.25 mm. Compounds were visualized using $KMnO_4$ stain [K_2CO_3 (40 g), $KMnO_4$ (6 g), and water (600 mL)] or CAM stain [Ce-$(NH_4)_4(SO_4)_4{\cdot}2H_2O$ (ceric ammonium sulfate: 10 g); ammonium molybdate (25 g); conc. H_2SO_4 (100 mL); and H_2O (900 mL)]. Preparative HPLC (Waters, 515 HPLC pump M; Waters, 515 HPLC pump L; Waters, 2767 sample manager; Waters SFO System Fluidics Organizer; Waters Acquity Ultra Performance LC, SQ Detector; Waters Binary Gradient Module) was performed on a Waters XBridgeTM column (5 μM C18, 150 × 19 mm). Diode detection was done between 210 and 600 nm. Gradient: ACN in (H_2O + 0.2% TFA). Chiral HPLC analysis was performed after benzoylation of the free amine on a Daicel Chiralpak AD column (250 × 4.5 mm, 10 μm particle size) using 10% isopropyl alcohol in hexane as an eluent (1.0 mL/min, UV-detection at 254 nm) and Rt = 15.1 min (*R*-enantiomer 12.8 min). High resolution mass spectra (HRMS) were recorded by direct injection on a q-TOF mass spectrometer (Synapt G2-Si) equipped with an electrospray ion source in positive mode with Leu-enkephalin (m/z = 556.2771) as an internal lock mass. The instrument was calibrated prior to measurement using the MS/MS spectrum of Glu-1-fibrinopeptide B.

General Procedure 1: Triphosgene Coupling of 2-Benzylpiperidine and Bis(4-fluorophenyl) Heterocycle. Triphosgene (0.7 equiv) was dissolved in dry DCM (0.1 M), and to this solution 2-benzylpiperidine (1 equiv) and Na_2CO_3 (1 equiv) were added at 0 °C. The mixture was stirred for 1 h, warming to RT. The mixture was then filtered and concentrated in vacuo. The residue was taken up in dry THF, followed by addition of a bis(4-fluoro-phenyl)heterocycle (1 equiv), DMAP (0.1 equiv), and DIPEA (1.1 equiv). The reaction mixture was refluxed to completion. The reaction was quenched with saturated NH_4Cl (aq), after which the water layer was extracted three times with EtOAc. The combined organic layers were washed with brine, dried with $MgSO_4$, and filtered and concentrated under reduced pressure.

*(R)-(2-Benzylpiperidin-1-yl)(4-(bis(4-fluorophenyl)(hydroxy)-methyl)-2H-1,2,3-triazol-2-yl)methanone (1) and (R)-(2-Benzylpiperidin-1-yl)(4-(bis(4-fluorophenyl)(hydroxy)methyl)-1H-1,2,3-triazol-1-yl)methanone (**2**).* Synthesized according to General Procedure 1 from **18** (123 mg, 0.428 mmol). The *N*1-isomer was isolated as first eluting isomer (1.63 mg, 3.3 μmol, 1.2%). ^{1}H NMR (400 MHz, $CDCl_3$): δ 7.41−6.57 (m, 14H), 4.76 (s, 1H), 4.40−4.18 (m, 1H), 3.56 (d, *J* = 66.9 Hz, 1H), 3.41−2.81 (m, 2H), 2.65 (s, 1H), 2.08−1.39 (m, 6H). Purity of > 95% as determined by LC/MS (Supporting Information). HRMS: calculated for $[C_{28}H_{26}F_2N_4O_2 + H]^+$ = 488.2079, found = 488.2090. *N*2-isomer (2.14 mg, 4.4 μmol, 1.5%): ^{1}H NMR (400 MHz, $CDCl_3$) δ 7.48 (s, 1H), 7.40−6.70 (m, 13H), 5.04−3.66 (m, 2H), 3.47 (s, 1H), 3.26 (t, *J* = 13.3 Hz, 1H), 3.16−2.81 (m, 2H), 1.94−1.43 (m, 6H). Purity of ≥ 95% as determined by LC/MS. HRMS: calculated for $[C_{28}H_{26}F_2N_4O_2{+}H]^+$ = 488.2079, found = 488.2091.

*(R)-(2-Benzylpiperidin-1-yl)(3-(bis(4-fluorophenyl)(hydroxy)-methyl)-1H-1,2,4-triazol-1-yl)methanone (**3**).* Synthesized according to General Procedure 1 from **21** (65 mg, 0.23 mmol). The title compound was obtained as a white solid (34.7 mg, 0.071 mmol, 35%). ^{1}H NMR (400 MHz, CD_3CN) δ 8.04 (bs, 1H), 7.35 (d, *J* = 6.6 Hz, 4H), 7.12 (s, 3H), 7.07−6.70 (m, 7H), 4.88 (s, 1H), 4.72 (s, 1H), 4.03 (d, *J* = 15.5 Hz, 1H), 3.23 (t, *J* = 13.1 Hz, 1H), 2.70 (s, 1H), 1.83−1.32 (m, 6H). Purity of ≥ 95% as determined by LC/MS. HRMS: calculated for $[C_{28}H_{26}F_2N_4O_2 + H]^+$ = 488.2097, found = 488.2096.

*(R)-(2-Benzylpiperidin-1-yl)(3-(bis(4-fluorophenyl)(hydroxy)-methyl)-1H-pyrazol-1-yl)methanone (**4**).* Synthesized according to General Procedure 1 from **25** (65 mg, 0.23 mmol). The title compound was obtained as a white solid (21 mg, 0.043 mmol, 21%). ^{1}H NMR (400 MHz, CD_3CN) δ 7.66−7.49 (m, 1H), 7.42−7.29 (m, 4H), 7.17 (dd, *J* = 5.1, 1.9 Hz, 3H), 7.13−6.92 (m, 6H), 6.22 (d, *J* = 2.6 Hz, 1H), 4.77 (s, 1H), 4.59 (s, 1H), 4.17−3.99 (m, 1H), 3.25 (td, *J* = 13.4, 3.0 Hz, 1H), 3.10 (dd, *J* = 13.5, 9.0 Hz, 1H), 2.83−2.68 (m, 1H), 1.88−1.21 (m, 6H). Purity of ≥ 95% as determined by LC/MS. HRMS: calculated for $[C_{29}H_{27}F_2N_3O_2 + H]^+$ = 488.2144, found = 488.2140.

*(R)-(2-Benzylpiperidin-1-yl)(4-(bis(4-fluorophenyl)(hydroxy)-methyl)-1H-imidazol-1-yl)methanone (**5**).* Synthesized according to General Procedure 1 from **29** (83 mg, 0.29 mmol). The title compound was obtained as a white solid (38 mg, 0.078 mmol, 27%). ^{1}H NMR (400 MHz, CD_3CN): δ 7.42 (s, 1H), 7.38−6.99 (m, 13H), 6.27 (s, 1H), 4.47 (s, 1H), 4.30 (qt, *J* = 7.1, 3.8 Hz, 1H), 3.81 (d, *J* = 13.7 Hz, 1H), 3.32 (td, *J* = 13.3, 2.9 Hz, 1H), 3.19 (dd, *J* = 13.7, 10.0 Hz, 1H), 2.78 (dd, *J* = 13.7, 5.5 Hz, 1H), 1.92−1.63 (m, 6H). Purity of ≥ 95% as determined by LC/MS. HRMS: calculated for $[C_{29}H_{27}F_2N_3O_2 + H]^+$ = 488.2144, found = 488.2142.

*tert-Butyl (S)-(1-(Methoxy(methyl)amino)-1-oxo-3-phenylpropan-2-yl)carbamic acid (**7**).* *N*-Boc-L-phenylalanine **6** (24.16 g, 91 mmol), *N*,*O*-dimethylhydroxylamine hydrochloride (9.95 g, 102 mmol), and 4-methylmorpholine (11.25 mL, 102 mmol) were dissolved in dichloromethane and cooled to 0 °C. EDCI-HCl (18.75 g, 98 mmol) was added in three portions with a 15 min interval. After consumption of the starting material, the reaction mixture was washed with satd aq. NH_4Cl, satd aq. $NaHCO_3$, and brine. The organic phase was dried ($MgSO_4$), filtered, and concentrated under reduced pressure to obtain the pure title compound as a honey like oil (25.9 g, 84 mmol, 92%). ^{1}H NMR (400 MHz, $CDCl_3$): δ 7.36−7.06 (m, 6H), 5.04−4.85 (m, 1H), 3.65 (s, 3H), 3.17 (s, 3H), 3.09−2.96 (m, 1H), 2.94−2.80 (m, 1H), 1.37 (s, 9H). ^{13}C NMR (101 MHz, $CDCl_3$): δ 155.27, 136.70, 129.56, 128.45, 126.86, 79.67, 61.65, 51.62, 43.93, 38.97, 28.42.

*tert-Butyl (S)-(1-Oxo-3-phenylpropan-2-yl)carbamate (**8**).* **7** (25.9 g, 84 mmol) was dissolved in THF and cooled to −15 °C. Subsequently, a 1 M solution of $LiAlH_4$ in THF (42 mL, 42 mmol) was added slowly. Upon completion, the reaction was quenched with 25% aq $KHSO_4$, allowed to warm up to RT, and stirred vigorously. Ethyl acetate was added, and the organic phase was separated, washed with satd aq. $NaHCO_3$ and brine, dried ($MgSO_4$), filtered, and concentrated under reduced pressure to give the title compound as a white solid (20.2 g, 81 mmol, 96%). ^{1}H NMR (400 MHz, $CDCl_3$): δ 9.63 (s, 1H), 7.43−7.04 (m, 5H), 5.18−4.99 (m, 1H), 4.43 (q, *J* = 6.8

DOI: 10.1021/acs.jmedchem.9b00686
J. Med. Chem. 2019, 62, 7910−7922

Hz, 1H), 3.12 (d, J = 6.7 Hz, 2H), 1.41 (s, 9H). ^{13}C NMR (101 MHz, $CDCl_3$): δ 199.56, 135.90, 129.46, 128.88, 127.19, 80.33, 60.91, 35.58, 28.39.

*tert-Butyl (S)-(1-Phenylbut-3-en-2-yl)carbamate (**9**).* To a solution of potassium bis(trimethylsilyl)amide (27 g, 135 mmol) in dry THF was added methyltriphenylphosphonium bromide (54.8 g, 153 mmol). The resulting mixture was stirred for 3 h and subsequently cooled to −78 °C, after which a solution of **8** (22.5 g, 90 mmol) in THF was added. The reaction was allowed to warm up to RT overnight and quenched with satd aq NH_4Cl. EtOAc was added, and the organic phase was separated, washed with satd aq. $NaHCO_3$ and brine, dried ($MgSO_4$), filtered, and concentrated under reduced pressure. The residue was purified with silica chromatography (8% ethyl acetate in petroleum ether) to give the desired product as a white, waxy solid (12.6 g, 50.9 mmol, 56%). ^{1}H NMR (400 MHz, $CDCl_3$): δ 7.34−7.13 (m, 5H), 5.88−5.71 (m, 1H), 5.16−5.03 (m, 2H), 4.45 (d, J = 27.0 Hz, 2H), 2.83 (d, J = 6.5 Hz, 2H), 1.40 (s, 9H). ^{13}C NMR (101 MHz, $CDCl_3$): δ 155.33, 138.18, 137.53, 129.68, 128.44, 126.59, 114.84, 79.53, 53.58, 41.60, 28.47.

*(S)-1-Phenylbut-3-en-2-amine (**10**).* **9** (9.7 g, 39.2 mmol) was dissolved in absolute methanol and 4 M aq HCl was added. After TLC showed full consumption of the starting material, the mixture was concentrated under reduced pressure and diluted with water. The solution was washed with diethyl ether and aq NaOH was used to make the aqueous layer basic (pH > 12). The aqueous phase was extracted 3× with chloroform. The organic layers were combined, dried ($MgSO_4$), filtered, and concentrated under reduced pressure to give the title compound in quantitative yield. The epimerised product that was formed during Wittig olefination was removed by recrystallization from toluene/*n*-propyl alcohol with *N*-acetyl-L-leucine according to the literature procedure,[49] yielding the amine as a yellow oil with an enantiomeric ratio of 97:3 as determined by chiral HPLC (*vide infra*). ^{1}H NMR (400 MHz, $CDCl_3$): δ 7.36−7.12 (m, 5H), 5.89 (ddd, J = 16.8, 10.3, 6.2 Hz, 1H), 5.14 (dt, J = 17.2, 1.5 Hz, 1H), 5.04 (dt, J = 10.3, 1.4 Hz, 1H), 3.64−3.52 (m, 1H), 2.83 (dd, J = 13.3, 5.4 Hz, 1H), 2.62 (dd, J = 13.3, 8.3 Hz, 1H), 1.31 (s, 3H). ^{13}C NMR (101 MHz, $CDCl_3$): δ 142.49, 138.86, 129.51, 128.50, 126.45, 113.77, 55.57, 44.43.

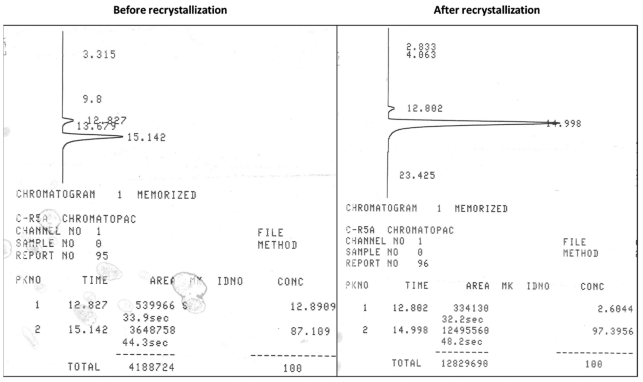

*(S)-2-Nitro-N-(1-phenylbut-3-en-2-yl)benzenesulfonamide (**11**).* **10** (3.5 g, 23.8 mmol), triethylamine (4.88 mL, 35.7 mmol), *N*,*N*-dimethylaminopyridine (1.45 g, 11.9 mmol) and 2-nitrobenzenesulphonyl chloride (6.85 g, 30.9 mmol) were dissolved in dry DCM and stirred overnight, after which the reaction mixture was concentrated under reduced pressure. Flash column chromatography (20% ethyl acetate in petroleum ether) yielded the desired product with trace impurities as an orange oil (6.7 g, 20 mmol, 85%). ^{1}H NMR (400 MHz, $CDCl_3$): δ 8.01−7.90 (m, 1H), 7.83−7.71 (m, 1H), 7.69−7.58 (m, 2H), 7.18−7.01 (m, 5H), 5.81−5.64 (m, 1H), 5.40 (d, J = 7.9 Hz, 1H), 5.13 (dt, J = 17.1, 1.2 Hz, 1H), 5.03 (dt, J = 10.3, 1.1 Hz, 1H), 4.32−4.17 (m, 1H), 2.92 (dd, J = 13.8, 6.1 Hz, 1H), 2.79 (dd, J = 13.8, 7.8 Hz, 1H). ^{13}C NMR (101 MHz, $CDCl_3$): δ 137.21, 136.22, 134.84, 133.22, 132.92, 130.79, 129.46, 128.54, 127.03, 125.53, 116.57, 58.68, 42.16.

*(S)-N-(But-3-en-1-yl)-2-nitro-N-(1-phenylbut-3-en-2-yl)-benzenesulfonamide (**12**).* **11** (6.7 g, 20.2 mmol) was dissolved in DMF, and K_2CO_3 (11.1 g, 81 mmol) and 4-bromo-1-butene (2.46 mL, 24.2 mmol) were added. The mixture was heated to 70 °C and stirred vigorously. After 24 h, an extra portion of 4-bromo-1-butene (2.46 mL, 24.2 mmol) was added and the resulting mixture was stirred for 72 h. The reaction was allowed to cool down to RT, diluted with brine, and extracted 3× with EtOAc. Combination, drying ($MgSO_4$), filtration, and concentration of the organic phases yielded the desired product as a brown oil (6.24 g, 16.2 mmol, 80%). ^{1}H NMR (400 MHz, $CDCl_3$): δ 7.92−7.84 (m, 1H), 7.69−7.52 (m, 3H), 7.25−7.12 (m, 5H), 5.89−5.64 (m, 2H), 5.17−5.02 (m, 4H), 4.72−4.62 (m, 1H), 3.50−3.31 (m, 2H), 3.08 (dd, J = 13.5, 5.9 Hz, 1H), 2.95 (dd, J = 13.5, 9.2 Hz, 1H), 2.50−2.31 (m, 2H). ^{13}C NMR (101 MHz, $CDCl_3$): δ 137.45, 135.28, 134.61, 134.09, 133.45, 131.70, 130.88, 129.39, 128.55, 126.75, 124.29, 118.98, 117.34, 61.66, 44.69, 39.60, 35.63.

*(S)-6-Benzyl-1-((2-nitrophenyl)sulfonyl)-1,2,3,6-tetrahydropyridine (**13**).* A solution of **12** (6.24 g, 16.2 mmol) in DCM was purged with argon, and a first generation Grubbs catalyst (400 mg, 3 mol %) was added. The mixture was heated to 40 °C and stirred overnight. Volatiles were removed under reduced pressure and flash column chromatography (40% diethyl ether in petroleum ether) yielded the desired product as brown powder (3.57 g, 9.96 mmol, 62%). ^{1}H NMR (400 MHz, $CDCl_3$): δ 7.85 (d, J = 7.7 Hz, 1H), 7.69−7.48 (m, 3H), 7.25−7.09 (m, 5H), 5.87−5.74 (m, 1H), 5.62 (d, J = 10.6 Hz, 1H), 4.56 (s, 1H), 3.93 (dd, J = 14.4, 6.2 Hz, 1H), 3.15 (ddd, J = 15.2, 11.7, 4.1 Hz, 1H), 3.00 (dd, J = 13.1, 6.0 Hz, 1H), 2.89 (dd, J = 13.1, 8.3 Hz, 1H), 2.21−2.04 (m, 1H), 1.93 (dt, J = 18.1, 5.0 Hz, 1H). ^{13}C NMR (101 MHz, $CDCl_3$): δ 137.28, 134.48, 133.30, 131.84, 130.44, 129.69, 128.50, 127.27, 126.79, 125.61, 124.27, 55.78, 41.71, 39.11, 24.33.

*(S)-6-Benzyl-1,2,3,6-tetrahydropyridine (**14**).* To a solution of thiophenol (2.56 mL, 24.9 mmol) in acetonitrile cooled with ice was added a 2 M aq solution of NaOH (12.45 mL, 24.9 mmol). After stirring for 10 min, the ice bath was removed and a solution of **13** (3.57 g, 9.96 mmol) in acetonitrile was added slowly. The resulting mixture was heated to 50 °C. When TLC showed full conversion of the starting material, the reaction was cooled to RT and diluted with aq HCl so that the pH was below 2. The aqueous layer was washed with Et_2O and diluted with aq NaOH until the pH was above 12. It was then extracted 3× with ethyl acetate. The organic layers were combined, dried ($MgSO_4$), filtered, and concentrated to afford the desired product as a yellow oil (1.71 g, 9.86 mmol, 99%). ^{1}H NMR (400 MHz, $CDCl_3$): δ 7.37−7.15 (m, 5H), 5.84−5.75 (m, 1H), 5.64 (dq, J = 10.1, 2.0 Hz, 1H), 3.61−3.51 (m, 1H), 3.17−2.99 (m, 1H), 2.85−2.75 (m, 2H), 2.70 (dd, J = 13.2, 8.8 Hz, 1H), 2.26−2.12 (m, 1H), 2.02−1.91 (m, 1H). ^{13}C NMR (101 MHz, $CDCl_3$): δ 138.97, 130.25, 129.39, 128.57, 126.43, 126.22, 55.47, 42.56, 42.12, 25.86.

*(R)-2-Benzylpiperidine (**15**).* In a three-neck flask containing two stoppers and one septum with empty balloons, **14** (1.70 g, 9.81 mmol) was dissolved in dichloroethane/methanol 10:3. This solution was purged with argon and cooled to 0 °C, after which $RuCl_3(H_2O)_3$ (257 mg, 0.98 mmol) was added. $NaBH_4$ (1.86 g, 49 mmol) was added quickly while capturing the formed H_2 gas in the empty balloons, thus keeping the reaction under hydrogen atmosphere. The reaction was allowed to warm up to RT and stirred overnight. Aqueous HCl was then added, so that the water layer had a pH of below 2. The aqueous layer was washed with Et_2O and diluted with aq NaOH until the pH was above 12. The water layer was extracted thrice with ethyl acetate. The organic layers were combined, dried ($MgSO_4$), filtered, and concentrated to yield the title compound as a yellow waxy solid (1.5 g, 8.6 mmol, 87%). ^{1}H NMR (400 MHz, $CDCl_3$): δ 7.38−7.03 (m, 5H), 3.08−2.89 (m, 1H), 2.77−2.64 (m, 2H), 2.64−2.46 (m, 2H), 1.84−1.73 (m, 1H), 1.73−1.63 (m, 1H), 1.63−1.52 (m, 1H), 1.52−1.38 (m, 1H), 1.37−1.15 (m, 3H). ^{13}C NMR (101 MHz, $CDCl_3$): δ 139.12, 129.23, 128.39, 126.20, 58.26, 47.08, 43.81, 32.77, 26.08, 24.80.

*Methyl 1H-1,2,3-Triazole-4-carboxylate (**17**).* This protocol was based on a literature procedure.[50] A mixture of azidotrimethylsilane (2.6 mL, 20 mmol) and methyl propiolate **16** (1.8 mL, 20 mmol) was heated for 4 h at 90 °C, concentrated, and coevaporated with MeOH

DOI: 10.1021/acs.jmedchem.9b00686
J. Med. Chem. 2019, 62, 7910−7922

to yield the title compound as a white solid (1.74 g, 14 mmol, 68%). ^{1}H NMR (400 MHz, MeOD): δ 8.35 (s, 1H), 3.92 (s, 3H). ^{13}C NMR (101 MHz, MeOD): δ 162.61, 139.63, 131.92, 52.53.

*Bis(4-fluorophenyl)(1H-1,2,3-triazol-4-yl)methanol (**18**).* **17** (100 mg, 0.787 mmol) was dissolved in THF and cooled to 0 °C. Under vigorous stirring, a 2 M solution of 4-fluorophenylmagnesium bromide in Et_2O (1.38 mL, 2.75 mmol) was added dropwise. The reaction mixture was allowed to warm up to RT and stirred overnight. The reaction was quenched with satd aq NH_4Cl. The aqueous phase was extracted with DCM (3×). The combined organic layers were dried ($MgSO_4$), filtered, and concentrated under reduced pressure. The residue was purified using flash column chromatography (40% to 60% ethyl acetate in pentane) in order to obtain the title compound as a white solid (210 mg, 0.731 mmol, 94%). ^{1}H NMR (400 MHz, MeOD): δ 7.60 (s, 1H), 7.45−7.33 (m, 4H), 7.15−6.98 (m, 4H).

*Methyl 1H-1,2,4-Triazole-3-carboxylate (**20**).* 1*H*-1,2,4-triazole-3-carboxylic acid **19** (250 mg, 2.21 mmol) was dissolved in MeOH (50 mL) and cooled to 0 °C. Thionyl chloride (0.48 mL, 6.6 mmol) was slowly added to the solution. The mixture was then heated to reflux for 3 h after which it was cooled to RT and concentrated in v:acuo to yield the title compound (271 mg, 2.14 mmol, 97%) as a white solid. ^{1}H NMR (400 MHz, MeOD): δ 9.24 (s, 1H), 4.05 (s, 3H).

*Bis(4-fluorophenyl)(1H-1,2,4-triazol-3-yl)methanol (**21**).* **20** (100 mg, 0.787 mmol) was dissolved in THF and cooled to 0 °C. Under vigorous stirring, a 2 M solution of 4-fluorophenylmagnesium bromide in Et_2O (1.37 mL, 2.75 mmol) was added dropwise. The reaction mixture was allowed to warm up to RT and stirred overnight. The reaction was quenched with satd aq NH_4Cl. The aqueous phase was extracted with ethyl acetate (3×). The combined organic layers were dried ($MgSO_4$), filtered, and concentrated under reduced pressure, yielding the title compound as an off-white solid (201 mg, 0.700 mmol, 89%). ^{1}H NMR (400 MHz, CD_3CN): δ 8.21 (s, 1H), 7.40 (dd, J = 8.7, 5.4 Hz, 4H), 7.08 (t, J = 8.7 Hz, 4H). ^{13}C NMR (101 MHz, MeOD): δ 163.23, 160.78, 140.15, 133.42, 128.89 (d, J = 8.2 Hz), 115.17, 114.42 (d, J = 21.7 Hz), 76.63.

*1H-Pyrazole-3-carboxylic acid (**23**).* Synthesis based on published procedure.[51] 3-Methyl-1*H*-pyrazole **22** (750 mg, 9.13 mmol) was dissolved in water, $KMnO_4$ (3.18 g, 20.1 mmol) was added, and the mixture was refluxed overnight. The reaction was cooled to room temperature, solids were filtered off, and the solvent was removed under reduced pressure. The resulting white powder was used directly without further purification.

*Ethyl 1H-Pyrazole-3-carboxylate (**24**).* Crude **23** was dissolved in anhydrous ethanol with a catalytic amount of concentrated H_2SO_4 and refluxed overnight. The reaction was allowed to cool to RT, the solvent was partially removed, and the residue was neutralized using satd aq $NaHCO_3$. The aqueous phase was extracted with ethyl acetate (3×), and the combined organic layers were dried ($MgSO_4$), filtered, and concentrated under reduced pressure, yielding the title compound as a white power (607 mg, 4.33 mmol, 47% over 2 steps). ^{1}H NMR (400 MHz, MeOD): δ 7.73 (d, J = 2.3 Hz, 1H), 6.85 (d, J = 2.3 Hz, 1H), 4.39 (q, J = 7.1 Hz, 2H), 1.40 (t, J = 7.1 Hz, 3H). ^{13}C NMR (101 MHz, MeOD): δ 108.84, 105.15, 61.94, 14.58.

*Bis(4-fluorophenyl)(1H-pyrazol-3-yl)methanol (**25**).* **24** (103 mg, 0.735 mmol) was dissolved in THF and cooled to 0 °C. Under vigorous stirring, a 2 M solution of 4-fluorophenylmagnesium bromide in Et_2O (1.29 mL, 2.57 mmol) was added dropwise. The reaction mixture was allowed to warm to RT and stirred overnight. The reaction was quenched with satd aq NH_4Cl. The aqueous phase was extracted with DCM (3×). Combined organic layers were dried ($MgSO_4$), filtered, and concentrated under reduced pressure. The residue was purified using silica flash chromatography (30% to 60% EtOAc in pentane) yielding the title compound as yellowish solid (175 mg, 0.611 mmol, 83%). ^{1}H NMR (400 MHz, $CDCl_3$): δ 8.08 (s, 1H), 7.24−7.10 (m, 5H), 7.03−6.85 (m, 4H), 5.83 (d, J = 2.2 Hz, 1H). ^{13}C NMR (101 MHz, MeOH): δ 162.18 (d, J = 246.8 Hz), 141.90 (d, J = 3.1 Hz), 131.77, 129.21 (d, J = 8.1 Hz), 114.90 (d, J = 21.4 Hz), 110.10, 105.43, 77.61.

*Ethyl 1-Trityl-1H-imidazole-4-carboxylate (**27**).* Ethyl 1*H*-imidazole-4-carboxylate **26** (100 mg, 0.714 mmol) was dissolved in DCM at 0 °C, after which trityl chloride (199 mg, 0.713 mmol) and triethylamine (0.117 mL, 0.856 mmol) were added. The reaction mixture was allowed to warm up to RT overnight, after which it was quenched with water. The organic phase was separated, dried ($MgSO_4$), filtered, and concentrated under reduced pressure, giving the title compound as a white powder (265 mg, 0.693 mmol, 97%). ^{1}H NMR (400 MHz, $CDCl_3$): δ 7.59 (d, J = 1.4 Hz, 1H), 7.45 (d, J = 1.4 Hz, 1H), 7.40−7.32 (m, 9H), 7.16−7.06 (m, 6H), 4.35 (q, J = 7.1 Hz, 2H), 1.37 (t, J = 7.1 Hz, 3H).

*Bis(4-fluorophenyl)(1-trityl-1H-imidazol-4-yl)methanol (**28**).* **27** (265 mg, 0.693 mmol) was dissolved in THF and cooled to 0 °C. Under vigorous stirring, a 2 M solution of 4-fluorophenylmagnesium bromide in Et_2O (1.38 mL, 2.75 mmol) was added dropwise. The reaction mixture was allowed to warm up to RT and further stirred overnight. The reaction was quenched with satd aq NH_4Cl. The aqueous phase was extracted 3× with ethyl acetate. The combined organic layers were dried ($MgSO_4$), filtered, and concentrated under reduced pressure. The residue was purified over silica column (50% EtOAc in pentane) in order to obtain the product as a yellowish powder (315 mg, 0.596 mmol, 86%). ^{1}H NMR (400 MHz, $CDCl_3$): δ 7.85 (s, 1H), 7.47−7.27 (m, 10H), 7.23−6.83 (m, 13H), 6.20 (s, 1H). ^{13}C NMR (101 MHz, $CDCl_3$): δ 162.18 (d, J = 246.9 Hz), 144.16, 140.79, 140.65, 129.62, 129.10 (d, J = 8.1 Hz), 128.92, 128.68, 121.17, 115.33, 115.28−114.61 (m), 76.24.

*Bis(4-fluorophenyl)(1H-imidazol-4-yl)methanol (**29**).* **28** (275 mg, 0.520 mmol) was dissolved in 50% TFA/DCM with a few milliliters of water and stirred overnight. Solvents were removed under reduced pressure, and the crude product was dissolved in diethyl ether and extracted with a 1 M aq HCl solution. The aqueous phase was made basic (pH > 12) with NaOH and extracted with ethyl acetate (3×). Combination, drying ($MgSO_4$), filtered, and concentration of the organic phases afforded a crude product that was of sufficient purity to use in subsequent reactions as judged by LC/MS (83 mg, 0.29 mmol, 56%).

*4-([1,1′-Biphenyl]-4-yl)-1H-1,2,3-triazole (**30**).* A mixture of formaldehyde (12.5 mL, 168 mmol), acetic acid (1.44 mL, 25.2 mmol), and 1,4-dioxane (125 mL) was stirred for 15 min. Sodium azide (1.64 g, 25.2 mmol) was added, followed by 4-ethynyl-1,1′-biphenyl (3.00 g, 16.8 mmol). After 10 min, sodium ascorbate (0.667 g, 3.37 mmol), and $CuSO_4 \cdot 5H_2O$ (0.210 g, 0.842 mmol) in 1 mL of water were added. The resulting mixture was stirred for 18 h at RT. It was diluted with H_2O (60 mL) and extracted with chloroform (3× 30 mL). The combined organic layers were dried ($MgSO_4$), filtered, and concentrated. The residue was suspended in 2 M NaOH (6 mL) and stirred for 20 h at RT. The reaction was acidified with 4 M HCl (aq), and the white precipitate was filtered off, yielding the desired product as a white solid (2.31 g, 10.4 mmol, 62%). ^{1}H NMR (400 MHz, DMSO): δ 15.18 (s, 1H), 8.40 (s, 1H), 7.99−7.93 (m, 2H), 7.81−7.75 (m, 2H), 7.75−7.69 (m, 2H), 7.53−7.45 (m, 2H), 7.42−7.34 (m, 1H). ^{13}C NMR (101 MHz, DMSO): δ 156.90, 145.31, 139.56, 128.99, 127.60, 127.17, 126.56, 126.09.

*(R,S)-2-Benzylpiperidine (**31**).* 2-Benzylpyridine (5.0 mL, 31 mmol) was dissolved in ethanol (100 mL), and concentrated aqueous HCl (10 mL) was added. Then PtO_2 (112 mg, 0.49 mmol) was added, and the mixture was shaken under a hydrogen atmosphere of 2 bar at RT. After overnight shaking, solids were filtered off over Celite. The solvent was removed under reduced pressure, and the residue was purified using flash column chromatography (10% methanol in DCM) to yield the title compound (4.2 g, 20 mmol, 64%). ^{1}H NMR (300 MHz, $CDCl_3$): δ 8.41 (s, 1H), 7.42−7.13 (m, 5H), 3.58−3.38 (m, 2H), 3.25−3.02 (m, 1H), 3.02−2.73 (m, 2H), 2.14−1.47 (m, 5H), 1.47−1.10 (m, 1H). ^{13}C NMR (75 MHz, $CDCl_3$): δ 136.16, 129.51, 128.76, 127.04, 58.59, 45.11, 40.07, 27.97, 22.61.

(4-([1,1′-Biphenyl]-4-yl)-1H-1,2,3-triazol-1-yl)(2-benzylpiperidin-1-yl)methanone (KT109). Synthesized according to General Procedure 1 from **30** (2.31 g, 10.4 mmol). The *N*1-isomer was isolated as the first eluting isomer (621 mg, 1.47 mmol, 14%). ^{1}H NMR (400 MHz, $CDCl_3$): δ 7.87 (s, 2H), 7.75−7.60 (m, 4H), 7.53−7.35 (m, 4H), 7.24 (d, J = 15.7 Hz, 6H), 4.86 (s, 1H), 4.37 (d, J = 13.5 Hz, 1H), 3.31 (d, J = 52.1 Hz, 2H), 2.70 (s, 1H), 2.11−1.62 (m,

DOI: 10.1021/acs.jmedchem.9b00686
J. Med. Chem. 2019, 62, 7910−7922

6H). Purity of ≥ 95% as determined by LC/MS (Supporting Information). HRMS: Calculated for $[C_{27}H_{26}N_4O + H]^+$ = 423.2179, found = 423.2183.

■ ASSOCIATED CONTENT

Supporting Information

The Supporting Information is available free of charge on the ACS Publications website at DOI: 10.1021/acs.jmedchem.9b00686.

Example DynaFit script, absorption, representative frames of molecular dynamics simulations, RMSD, contact maps, potential energy, summary of molecular dynamics interactions, synthesis scheme, and LC/MS traces showing purity of biochemically profiled final compounds (PDF)

Molecular Formula Strings (CSV)

Compound 1 bound to DAGL-alpha homology model (Figure 4) (PDB)

Compound 2 bound to DAGL-alpha homology model (Supporting Figure 3A) (PDB)

Compound 3 bound to DAGL-alpha homology model (Supporting Figure 3B) (PDB)

Compound 4 bound to DAGL-alpha homology model (Supporting Figure 3C) (PDB)

Compound 5 bound to DAGL-alpha homology model (PDB)

■ AUTHOR INFORMATION

Corresponding Author

*E-mail: m.van.der.stelt@chem.leidenuniv.nl. Tel: (+31)71 527 4768.

ORCID

Antonius P.A. Janssen: 0000-0003-4203-261X

Hui Deng: 0000-0003-0899-4188

Mario van der Stelt: 0000-0002-1029-5717

Author Contributions

APAJ, JvH, OJMB, and HD designed and performed the experiments. APAJ, JvH, OJMB, GJPvW, and MvdS interpreted the results. APAJ, OJMB, GJPvW, and MvdS wrote the paper.

Notes

The authors declare no competing financial interest.

■ ACKNOWLEDGMENTS

A.M.C.H. van Nieuwendijk is kindly acknowledged for his advice on the synthesis and his help in the chiral HPLC work. APAJ acknowledges the NWO ECHO-grant 711.014.009 for funding.

■ ABBREVIATIONS USED

DAGL, diacylglycerol lipase; FAAH, fatty acid amide hydrolase; MAGL, monoacylglycerol lipase; ABHD, α/β-hydrolase domain containing protein; DDHD2, DDHD domain containing protein; DIPEA, diisopropylethylamine; KHMDS, potassium bis(trimethylsilyl) amide; EDCI, *N*-(3-(dimethylamino)propyl)-*N*′-ethylcarbodiimide hydrochloride; Ns, nosyl; PNPB, para-nitrophenylbutyrate; N.D., not determined

■ REFERENCES

(1) Zhao, Z.; Bourne, P. E. Progress with Covalent Small-Molecule Kinase Inhibitors. *Drug Discovery Today* **2018**, *23* (3), 727−735.

(2) Singh, J.; Petter, R. C.; Baillie, T. a; Whitty, A. The Resurgence of Covalent Drugs. *Nat. Rev. Drug Discovery* **2011**, *10* (4), 307−317.

(3) Keith, J. M.; Jones, W. M.; Tichenor, M.; Liu, J.; Seierstad, M.; Palmer, J. A.; Webb, M.; Karbarz, M.; Scott, B. P.; Wilson, S. J.; Luo, L.; Wennerholm, M. L.; Chang, L.; Rizzolio, M.; Rynberg, R.; Chaplan, S. R.; Breitenbucher, J. G. Preclinical Characterization of the FAAH Inhibitor JNJ-42165279. *ACS Med. Chem. Lett.* **2015**, *6* (12), 1204−1208.

(4) Postnov, A.; Schmidt, M. E.; Pemberton, D. J.; de Hoon, J.; van Hecken, A.; van den Boer, M.; Zannikos, P.; van der Ark, P.; Palmer, J. A.; Rassnick, S.; Celen, S.; Bormans, G.; van Laere, K. Fatty Acid Amide Hydrolase Inhibition by JNJ-42165279: A Multiple-Ascending Dose and a Positron Emission Tomography Study in Healthy Volunteers. *Clin. Transl. Sci.* **2018**, *11* (4), 397−404.

(5) Johnson, D. S.; Stiff, C.; Lazerwith, S. E.; Kesten, S. R.; Fay, L. K.; Morris, M.; Beidler, D.; Liimatta, M. B.; Smith, S. E.; Dudley, D. T.; Sadagopan, N.; Bhattachar, S. N.; Kesten, S. J.; Nomanbhoy, T. K.; Cravatt, B. F.; Ahn, K. Discovery of PF-04457845: A Highly Potent, Orally Bioavailable, and Selective Urea FAAH Inhibitor. *ACS Med. Chem. Lett.* **2011**, *2* (2), 91−96.

(6) Huggins, J. P.; Smart, T. S.; Langman, S.; Taylor, L.; Young, T. An Efficient Randomised, Placebo-Controlled Clinical Trial with the Irreversible Fatty Acid Amide Hydrolase-1 Inhibitor PF-04457845, Which Modulates Endocannabinoids but Fails to Induce Effective Analgesia in Patients with Pain Due to Osteoarthritis of Th. *Pain* **2012**, *153* (9), 1837−1846.

(7) Cisar, J. S.; Weber, O. D.; Clapper, J. R.; Blankman, J. L.; Henry, C. L.; Simon, G. M.; Alexander, J. P.; Jones, T. K.; Ezekowitz, R. A. B.; O'Neill, G. P.; Grice, C. A. Identification of ABX-1431, a Selective Inhibitor of Monoacylglycerol Lipase and Clinical Candidate for Treatment of Neurological Disorders. *J. Med. Chem.* **2018**, *61* (20), 9062−9084.

(8) Fraser, I.; Blankman, J.; Clapper, J.; Grice, C.; O'Neill, G.; Ezekowitz, A.; Thurston, A.; Geenens, E.; Vandermeulen, C.; de Hoon, J. Preclinical Characterization and First-in-Human Administration of a Selective Monoacylglycerol Lipase Inhibitor, ABX-1431. In *Front. Pharmacol. Conference Abstract: EUFEMED* 2017; DOI: 10.3389/conf.fphar.2017.62.00011.

(9) Copeland, R. A. *Evaluation of Enzyme Inhibitors in Drug Discovery: A Guide for Medicinal Chemists and Pharmacologists*; Wiley, 2013.

(10) Schwartz, P. A.; Kuzmic, P.; Solowiej, J.; Bergqvist, S.; Bolanos, B.; Almaden, C.; Nagata, A.; Ryan, K.; Feng, J.; Dalvie, D.; Kath, J. C.; Xu, M.; Wani, R.; Murray, B. W. Covalent EGFR Inhibitor Analysis Reveals Importance of Reversible Interactions to Potency and Mechanisms of Drug Resistance. *Proc. Natl. Acad. Sci. U. S. A.* **2014**, *111* (1), 173−178.

(11) Aaltonen, N.; Savinainen, J. R.; Ribas, C. R.; Rönkkö, J.; Kuusisto, A.; Korhonen, J.; Navia-Paldanius, D.; Häyrinen, J.; Takabe, P.; Käsnänen, H.; Pantsar, T.; Laitinen, T.; Lehtonen, M.; Pasonen-Seppänen, S.; Poso, A.; Nevalainen, T.; Laitinen, J. T. Piperazine and Piperidine Triazole Ureas as Ultrapotent and Highly Selective Inhibitors of Monoacylglycerol Lipase. *Chem. Biol.* **2013**, *20* (3), 379−390.

(12) van Esbroeck, A. C. M.; Janssen, A. P. A.; Cognetta, A. B.; Ogasawara, D.; Shpak, G.; van der Kroeg, M.; Kantae, V.; Baggelaar, M. P.; de Vrij, F. M. S.; Deng, H.; Allarà, M.; Fezza, F.; Lin, Z.; van der Wel, T.; Soethoudt, M.; Mock, E. D.; den Dulk, H.; Baak, I. L.; Florea, B. I.; Hendriks, G.; De Petrocellis, L.; Overkleeft, H. S.; Hankemeier, T.; De Zeeuw, C. I.; Di Marzo, V.; Maccarrone, M.; Cravatt, B. F.; Kushner, S. A.; van der Stelt, M. Activity-Based Protein Profiling Reveals off-Target Proteins of the FAAH Inhibitor BIA 10−2474. *Science* **2017**, *356* (6342), 1084−1087.

(13) Kerbrat, A.; Ferré, J.-C; Fillatre, P.; Ronzière, T.; Vannier, S.; Carsin-Nicol, B.; Lavoué, S.; Vérin, M.; Gauvrit, J.-Y; Le Tulzo, Y.;

Edan, G. Acute Neurologic Disorder from an Inhibitor of Fatty Acid Amide Hydrolase. *N. Engl. J. Med.* **2016**, *375* (18), 1717−1725.
(14) Miyahisa, I.; Sameshima, T.; Hixon, M. S. Rapid Determination of the Specificity Constant of Irreversible Inhibitors (k Inact/K I) by Means of an Endpoint Competition Assay. *Angew. Chem., Int. Ed.* **2015**, *54* (47), 14099−14102.
(15) Ahn, K.; Smith, S. E.; Liimatta, M. B.; Beidler, D.; Sadagopan, N.; Dudley, D. T.; Young, T.; Wren, P.; Zhang, Y.; Swaney, S.; Van Becelaere, K.; Blankman, J. L.; Nomura, D. K.; Bhattachar, S. N.; Stiff, C.; Nomanbhoy, T. K.; Weerapana, E.; Johnson, D. S.; Cravatt, B. F. Mechanistic and Pharmacological Characterization of PF-04457845: A Highly Potent and Selective Fatty Acid Amide Hydrolase Inhibitor That Reduces Inflammatory and Noninflammatory Pain. *J. Pharmacol. Exp. Ther.* **2011**, *338* (1), 114−124.
(16) Strelow, J. M. A Perspective on the Kinetics of Covalent and Irreversible Inhibition. *SLAS Discovery Adv. Life Sci. R&D* **2017**, *22* (1), 3−20.
(17) Bisogno, T.; Howell, F.; Williams, G.; Minassi, A.; Cascio, M. G.; Ligresti, A.; Matias, I.; Schiano-Moriello, A.; Paul, P.; Williams, E.-J; Gangadharan, U.; Hobbs, C.; Di Marzo, V.; Doherty, P. Cloning of the First Sn1-DAG Lipases Points to the Spatial and Temporal Regulation of Endocannabinoid Signaling in the Brain. *J. Cell Biol.* **2003**, *163* (3), 463−468.
(18) Janssen, F. J.; van der Stelt, M. Inhibitors of Diacylglycerol Lipases in Neurodegenerative and Metabolic Disorders. *Bioorg. Med. Chem. Lett.* **2016**, *26* (16), 3831−3837.
(19) Baggelaar, M. P.; Maccarrone, M.; van der Stelt, M. 2-Arachidonoylglycerol: A Signaling Lipid with Manifold Actions in the Brain. *Prog. Lipid Res.* **2018**, *71*, 1−17.
(20) Ogasawara, D.; Deng, H.; Viader, A.; Baggelaar, M. P.; Breman, A.; den Dulk, H.; van den Nieuwendijk, A. M. C. H.; Soethoudt, M.; van der Wel, T.; Zhou, J.; Overkleeft, H. S.; Sanchez-Alavez, M.; Mori, S.; Nguyen, W.; Conti, B.; Liu, X.; Chen, Y.; Liu, Q.; Cravatt, B. F.; van der Stelt, M. Rapid and Profound Rewiring of Brain Lipid Signaling Networks by Acute Diacylglycerol Lipase Inhibition. *Proc. Natl. Acad. Sci. U. S. A.* **2016**, *113* (1), 26−33.
(21) Hsu, K.-L; Tsuboi, K.; Chang, J. W.; Whitby, L. R.; Speers, A. E.; Pugh, H.; Cravatt, B. F. Discovery and Optimization of Piperidyl-1,2,3-Triazole Ureas as Potent, Selective, and in Vivo-Active Inhibitors of α/β-Hydrolase Domain Containing 6 (ABHD6). *J. Med. Chem.* **2013**, *56* (21), 8270−8279.
(22) Baggelaar, M. P.; Chameau, P. J. P.; Kantae, V.; Hummel, J.; Hsu, K.-L; Janssen, F.; van der Wel, T.; Soethoudt, M.; Deng, H.; den Dulk, H.; Allarà, M.; Florea, B. I.; Di Marzo, V.; Wadman, W. J.; Kruse, C. G.; Overkleeft, H. S.; Hankemeier, T.; Werkman, T. R.; Cravatt, B. F.; van der Stelt, M. Highly Selective, Reversible Inhibitor Identified by Comparative Chemoproteomics Modulates Diacylglycerol Lipase Activity in Neurons. *J. Am. Chem. Soc.* **2015**, *137* (27), 8851−8857.
(23) Adibekian, A.; Hsu, K.-L.; Speers, A. E.; Brown, S. J.; Spicer, T.; Fernandez-Vega, V.; Ferguson, J.; Cravatt, B. F.; Hodder, P.; Rosen, H. Optimization and Characterization of a Triazole Urea Inhibitor for Alpha/Beta Hydrolase Domain-Containing Protein 11 (ABHD11): Anti-Probe for LYPLA1/LYPLA2 Dual Inhibitor ML211; *National Center for Biotechnology Information (US)*, **2010**.
(24) Inloes, J. M.; Hsu, K.-L; Dix, M. M.; Viader, A.; Masuda, K.; Takei, T.; Wood, M. R.; Cravatt, B. F. The Hereditary Spastic Paraplegia-Related Enzyme DDHD2 Is a Principal Brain Triglyceride Lipase. *Proc. Natl. Acad. Sci. U. S. A.* **2014**, *111* (41), 14924−14929.
(25) Brindisi, M.; Maramai, S.; Gemma, S.; Brogi, S.; Grillo, A.; Di Cesare Mannelli, L.; Gabellieri, E.; Lamponi, S.; Saponara, S.; Gorelli, B.; Tedesco, D.; Bonfiglio, T.; Landry, C.; Jung, K.-M; Armirotti, A.; Luongo, L.; Ligresti, A.; Piscitelli, F.; Bertucci, C.; Dehouck, M.-P; Campiani, G.; Maione, S.; Ghelardini, C.; Pittaluga, A.; Piomelli, D.; Di Marzo, V.; Butini, S. Development and Pharmacological Characterization of Selective Blockers of 2-Arachidonoyl Glycerol Degradation with Efficacy in Rodent Models of Multiple Sclerosis and Pain. *J. Med. Chem.* **2016**, *59* (6), 2612−2632.
(26) Hsu, K.-L; Tsuboi, K.; Whitby, L. R.; Speers, A. E.; Pugh, H.; Inloes, J.; Cravatt, B. F. Development and Optimization of Piperidyl-1,2,3-Triazole Ureas as Selective Chemical Probes of Endocannabinoid Biosynthesis. *J. Med. Chem.* **2013**, *56* (21), 8257−8269.
(27) Deng, H.; Kooijman, S.; van den Nieuwendijk, A. M. C. H.; Ogasawara, D.; van der Wel, T.; van Dalen, F.; Baggelaar, M. P.; Janssen, F. J.; van den Berg, R. J. B. H. N.; den Dulk, H.; Cravatt, B. F.; Overkleeft, H. S.; Rensen, P. C. N.; van der Stelt, M. Triazole Ureas Act as Diacylglycerol Lipase Inhibitors and Prevent Fasting-Induced Refeeding. *J. Med. Chem.* **2017**, *60* (1), 428−440.
(28) Clayden, J.; Greeves, N.; Warren, S. Nucleophilic Substitution at the Carbonyl Group. In *Organic Chemistry*; Oxford University Press, 2012; pp 197−221.
(29) Blais, M.-J; Enea, O.; Berthon, G. Relations Structure-Réactivité Grandeurs Thermodynamiques de Protonation d'h'et'erocycles Saturés et Non Saturés. *Thermochim. Acta* **1977**, *20* (3), 335−345.
(30) Catalan, J.; Claramunt, R. M.; Elguero, J.; Laynez, J.; Menendez, M.; Anvia, F.; Quian, J. H.; Taagepera, M.; Taft, R. W. Basicity and Acidity of Azoles: The Annelation Effect in Azoles. *J. Am. Chem. Soc.* **1988**, *110* (13), 4105−4111.
(31) Hansen, L. D.; West, B. D.; Baca, E. J.; Blank, C. L. Thermodynamics of Proton Ionization from Some Substituted 1,2,3-Triazoles in Dilute Aqueous Solution. *J. Am. Chem. Soc.* **1968**, *90* (24), 6588−6592.
(32) Baggelaar, M. P.; Janssen, F. J.; van Esbroeck, A. C. M.; den Dulk, H.; Allarà, M.; Hoogendoorn, S.; McGuire, R.; Florea, B. I.; Meeuwenoord, N.; van den Elst, H.; van der Marel, G. A.; Brouwer, J.; Di Marzo, V.; Overkleeft, H. S.; van der Stelt, M. Development of an Activity-Based Probe and In Silico Design Reveal Highly Selective Inhibitors for Diacylglycerol Lipase-α in Brain. *Angew. Chem., Int. Ed.* **2013**, *52* (46), 12081−12085.
(33) Zhao, K.-Y; Tsou, C.-L Kinetics of Substrate Reaction during Irreversible Modification of Enzyme Activity Where the Modifier Is Not in Great Excess of the Enzyme. *J. Theor. Biol.* **1992**, *157* (4), 505−521.
(34) Maurer, T. S.; Fung, H.-L Comparison of Methods for Analyzing Kinetic Data from Mechanism-Based Enzyme Inactivation: Application to Nitric Oxide Synthase. *AAPS PharmSci* **2000**, *2* (1), 68−77.
(35) Krippendorff, B.-F; Neuhaus, R.; Lienau, P.; Reichel, A.; Huisinga, W. Mechanism-Based Inhibition: Deriving K(I) and k(Inact) Directly from Time-Dependent IC(50) Values. *J. Biomol. Screening* **2009**, *14* (8), 913−923.
(36) Kuzmič, P. Program DYNAFIT for the Analysis of Enzyme Kinetic Data: Application to HIV Proteinase. *Anal. Biochem.* **1996**, *237* (2), 260−273.
(37) Kuzmič, P. DynaFit–a Software Package for Enzymology. *Methods Enzymol.* **2009**, *467* (C), 247−280.
(38) Hsu, K. L.; Tsuboi, K.; Adibekian, A.; Pugh, H.; Masuda, K.; Cravatt, B. F. DAGLβ Inhibition Perturbs a Lipid Network Involved in Macrophage Inflammatory Responses. *Nat. Chem. Biol.* **2012**, *8* (12), 999−1007.
(39) Mileni, M.; Johnson, D. S.; Wang, Z.; Everdeen, D. S.; Liimatta, M.; Pabst, B.; Bhattacharya, K.; Nugent, R. A.; Kamtekar, S.; Cravatt, B. F.; Ahn, K.; Stevens, R. C. Structure-Guided Inhibitor Design for Human FAAH by Interspecies Active Site Conversion. *Proc. Natl. Acad. Sci. U. S. A.* **2008**, *105* (35), 12820−12824.
(40) Edwards, P. D.; Meyer, E. F.; Vijayalakshmi, J.; Tuthill, P. A.; Andisik, D. A.; Gomes, B.; Strimpler, A. Design, Synthesis, and Kinetic Evaluation of a Unique Class of Elastase Inhibitors, the Peptidyl α-Ketobenzoxazoles, and the x-Ray Crystal Structure of the Covalent Complex between Porcine Pancreatic Elastase and Ac-Ala-Pro-Val-2-Benzoxazole. *J. Am. Chem. Soc.* **1992**, *114* (5), 1854−1863.
(41) Janssen, F. J.; Baggelaar, M. P.; Hummel, J. J. A.; Overkleeft, H. S.; Cravatt, B. F.; Boger, D. L.; van der Stelt, M. Comprehensive Analysis of Structure−Activity Relationships of α-Ketoheterocycles as Sn-1-Diacylglycerol Lipase α Inhibitors. *J. Med. Chem.* **2015**, *58* (24), 9742−9753.

DOI: 10.1021/acs.jmedchem.9b00686
J. Med. Chem. 2019, 62, 7910−7922

(42) *Schrödinger*, release 2018−3, LigPrep; Schrödinger, LLC: New York, NY, 2018.
(43) *Schrödinger*, release 2018−3, Epik; Schrödinger, LLC, New York, NY, 2018.
(44) Harder, E.; Damm, W.; Maple, J.; Wu, C.; Reboul, M.; Xiang, J. Y.; Wang, L.; Lupyan, D.; Dahlgren, M. K.; Knight, J. L.; Kaus, J. W.; Cerutti, D. S.; Krilov, G.; Jorgensen, W. L.; Abel, R.; Friesner, R. A. OPLS3: A Force Field Providing Broad Coverage of Drug-like Small Molecules and Proteins. *J. Chem. Theory Comput.* **2016**, *12* (1), 281−296.
(45) *Small-Molecule Drug Discovery Suite 2018*−3; Schrödinger, LLC: New York, NY, 2018.
(46) *Schrödinger*, release 2018−3, Desmond Molecular Dynamics System; D. E. Shaw Research: New York, NY, 2018. *Maestro-Desmond Interoperability Tools*; Schrödinger, New York, NY, 2018.
(47) Berendsen, H. J. C.; Postma, J. P. M.; van Gunsteren, W. F.; Hermans, J. *Intermolecular Forces*; Pullman, B., Ed. Reidel Publishing Company: Dordrecht, 1981.
(48) Gottlieb, H. E.; Kotlyar, V.; Nudelman, A. NMR Chemical Shifts of Common Laboratory Solvents as Trace Impurities. *J. Org. Chem.* **1997**, *62* (21), 7512−7515.
(49) Blacker, A. J.; Roy, M.; Hariharan, S.; Headley, C.; Upare, A.; Jagtap, A.; Wankhede, K.; Mishra, S. K.; Dube, D.; Bhise, S.; Vishwasrao, S.; Kadam, N. Convenient Method for Synthesis of N-Protected α-Amino Epoxides: Key Intermediates for HIV Protease Inhibitors. *Org. Process Res. Dev.* **2011**, *15* (2), 331−338.
(50) Taherpour, A. A.; Kheradmand, K. One-Pot Microwave-Assisted Solvent Free Synthesis of Simple Alkyl 1,2,3-Triazole-4-Carboxylates by Using Trimethylsilyl Azide. *J. Heterocycl. Chem.* **2009**, *46* (1), 131−133.
(51) Fatin-Rouge, N.; Tóth, É.; Perret, D.; Backer, R. H.; Merbach, A. E.; Bünzli, J.-C. G. Lanthanide Podates with Programmed Intermolecular Interactions: Luminescence Enhancement through Association with Cyclodextrins and Unusually Large Relaxivity of the Gadolinium Self-Aggregates. *J. Am. Chem. Soc.* **2000**, *122* (44), 10810−10820.

DOI: 10.1021/acs.jmedchem.9b00686
J. Med. Chem. 2019, 62, 7910−7922